P9.6 RADAR OBSERVATIONS OF A TORNADIC SEVERE FRONTAL RAINBAND

Jenni Rauhala* and Ari-Juhani Punkka
Finnish Meteorological Institute, Helsinki, Finland

1. INTRODUCTION

On the afternoon of 26 August 2005, severe convective storms caused vast wind damage in western Finland: 382 wind damage or flood reports and 9 tornado cases (Fig. 1). Two rainbands developed over western Finland: while, the pre-frontal rainband caused minor flooding, almost all of the observed severe weather (Fig. 1) occurred along the second rainband associated with a cold front.

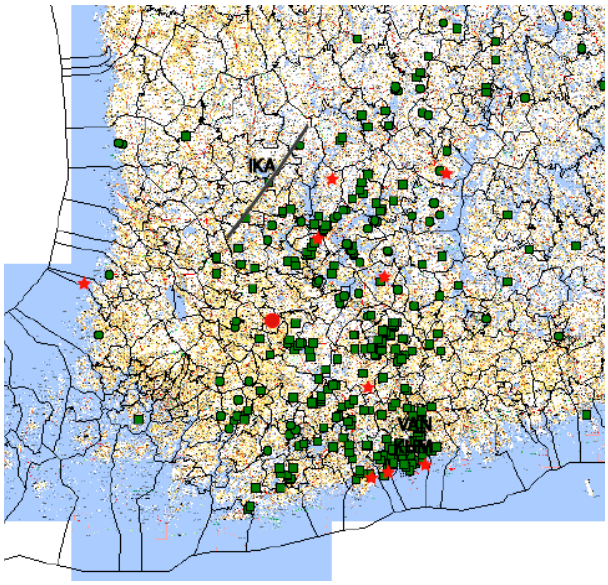

Fig. 1. Emergency reports of wind damage (green squares and dots) and tornado reports (red stars) on 26 August 2005 in western Finland. The red circle indicates the location of the Jokioinen sounding station and IKA, VAN and KUM, the location of Ikaalinen, Vantaa and Kumpula radars, respectively. The gray line denotes a mesovortex path identified by the radar.

During the event, the Finnish Meteorological Institute's (FMI) operational nowcasting radar products did not indicate many features along the severe frontal rainband that would specifically attract the attention of a forecaster for tornado potential. The storms were shallow, not very intense in reflectivity and there was no lightning. Moreover, another rainband with lightning, more intense radar echoes and higher storm tops preceded the frontal rainband capturing the forecasters' attention. The cold pool of the prefrontal rainband had cooled and moistened boundary-layer air ahead of the frontal rainband, which complicated the nowcasting of severe weather. Although a warning for thunderstorm wind gusts was issued well before the onset of the event, the magnitude of the damage was not anticipated by FMI forecasters.

A closer look into radar reflectivity and velocity patterns indicated small scale bowing segments in the reflectivity fields co-located with mesovortices, similar to those shown in previous studies (e.g. Weisman and Trapp 2003) to be capable of producing both straight-line wind damage and tornadoes. The storm environment, with significant low level vertical wind shear, had likely influenced the mesovortex formation. Fortunately, some of these mesovortices occurred near a polarimetric radar, which offered insight into their small scale precipitation structures.

2. DATA

The case occurred partly over the Helsinki Testbed mesoscale observation network area (Saltikoff et al. 2005) during the August 2005 campaign period. The radar analysis was based on data from two 5.32 cm Doppler radars of the FMI and the polarimetric radar of the University of Helsinki. The lowest elevations were not used for velocity analysis because of velocity folding. Complete volume scans from FMI radars and the Kumpula radar were available for 5-minute and 10-minute intervals, respectively. The analysis of these data suffers from the poor scanning intervals and the several minutes' time difference between different parameters. In this study, the length of the sample volume of all processed radar pictures was of 139 m.

The wind damage reports were obtained from the Ministry of Interior's Emergency Response Centres. The tornado reports had been collected by FMI, and 6 of them have been confirmed.

3. THE STORM ENVIRONMENT

On 26 August, a 500-hPa short wave trough was approaching southern Finland from southwest. A surface low centre that was in the morning over central Sweden, was deepening and moving northwards during 26 August. At 1200 UTC (Fig. 2) the cold front was situated west of Finland and moving northeast. In the warm sector, a southerly mid-level jet was present, which descended and intensified ahead of the cold front during late afternoon (not shown).

The Jokioinen 1200 UTC sounding was released between pre-frontal and frontal rainbands (Fig. 3). The sounding had very low CAPE values and a weak capping inversion at the 925 hPa level. The low level humidity was in shallow layer just above the surface.

* *Corresponding author address:* Jenni Rauhala, Finnish Meteorological Institute, Meteorological Applications, P.O.BOX 503, 00101 Helsinki, Finland; e-mail: jenni.rauhala@fmi.fi

The wind profile was characterized by a very high low level wind shear (bulk shear of 18.1 m/s in the 0-1 km layer) and a wind maximum of 28 m/s at 2.5 km height. According to numerical simulations by Weisman and Trapp (2003), low level mesoscale vortices are readily produced in squall lines developing with a moderate-to-strong environmental vertical wind shear.

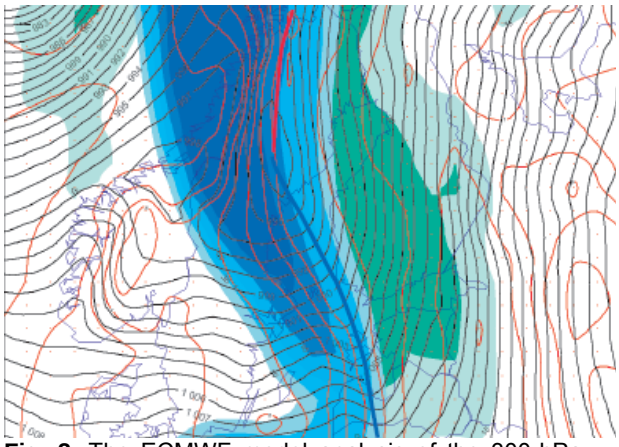

Fig. 2. The ECMWF model analysis of the 300-hPa (blue≥30 m/s) and 850-hPa (green≥15 m/s) wind speed, 850-hPa temperature (red lines) and surface isobars (black lines) at 1200 UTC with manual frontal analysis.

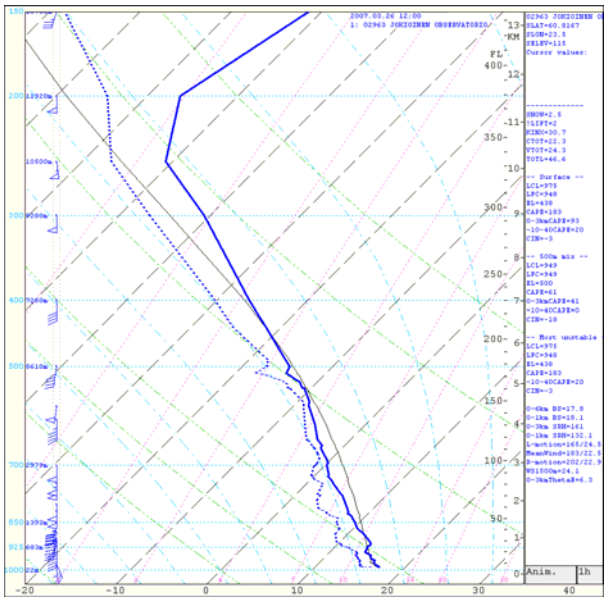

Fig. 3. The observed sounding at Jokioinen at 1200 UTC (blue) and the surface parcel in black.

The surface observations (not shown) showed that the pre-frontal rainband caused a temperature drop, but the dewpoint temperatures increased. The surface air was nearly saturated between the rainbands. The satellite pictures showed that this area was overcast. Lightning occurred in the pre-frontal rainband but there were no lightning along the cold frontal rainband.

The synoptic-scale environment of this case resembles the dynamic pattern associated with bow echo development as described by Johns (1993). In terms of dynamic pattern, a squall line usually develops along or ahead of a cold front with embedded bow echoes. According to Przybylinski (1995), the embedded small scale (less than 20 km wide) bow echoes can be significant initiators of wind and tornadoes in a cool season dynamic pattern. The pattern is usually characterised by an almost parallel orientation of the low-level jet with respect to mid- and upper-level jets and strong vertical wind shear. However, as noted by Johns (1993), the instability can vary in this pattern from extremely unstable to marginally unstable. A common feature for this pattern was, though, a dry layer in the downdraft entrainment region (3-7 km AGL). This dry region was not observed in the pre-squall line sounding (Fig. 3) or in the (overcast) satellite pictures.

Squall lines producing both tornadoes and wind damage have been documented earlier in similar environments (e.g. Carbone 1982, Funk at al. 1999). However, our case had only marginal CAPE.

4. RADAR OBSERVATIONS

4.1 Ikaalinen Doppler radar observations

The severe frontal rainband moved fast, 15 m/s, northeastwards. At around 1300 UTC, the orientation of the rainband changed from north-south to northwest-southeast and it became more perpendicular to the low level wind shear. The low level reflectivity gradient was sharp in leading line and several weak echo channels were observed behind it (Fig. 4a-d). The connection between the weak echo channels and the rear-inflow jet is supported by 22 m/s velocity maxima behind and perpendicular to the leading line (Fig. 4g-h).

The breaking of the convective line into gaps in reflectivity was observed. These gaps occurred at about a 15 km distance from each other and were characterized in PPI pictures by rainband bulges of lower reflectivity surrounded by higher reflectivities. The maximum reflectivities throughout the radar volume (50-55 dBZ) were located close to these low level reflectivity gaps. Also the 15 dBZ storm tops were below 5 km. The rainband bulges lasted at least the studied time 1420-1555 UTC. During that time there was no substantial changes in the radar reflectivity structure.

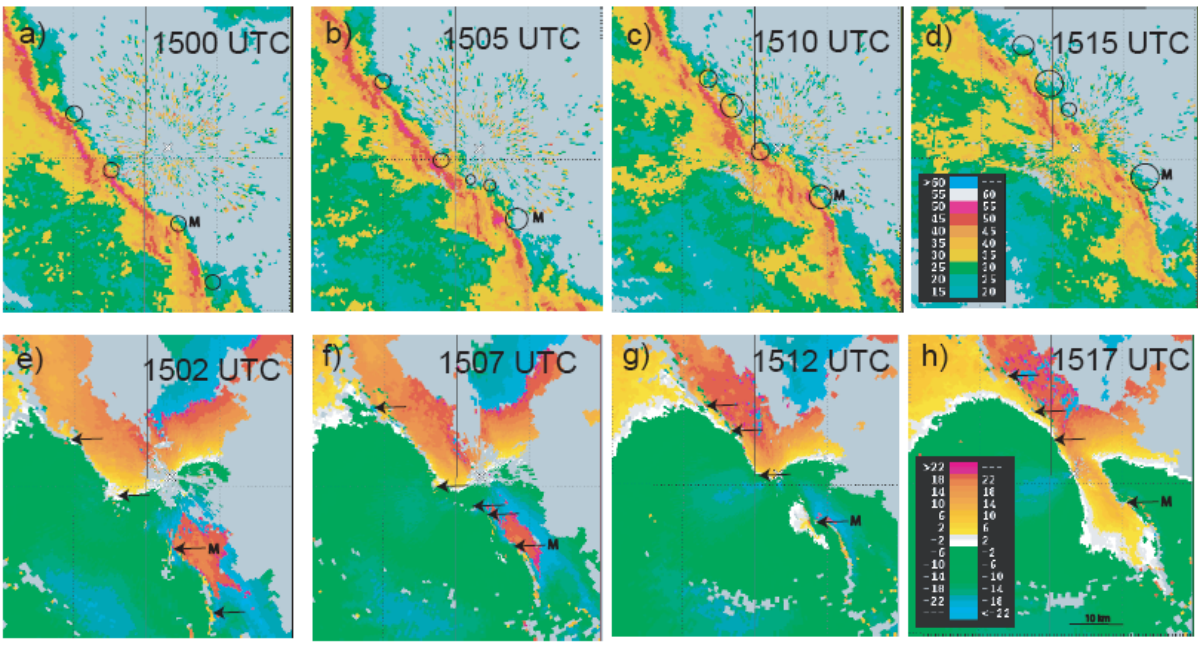

Fig. 4. Ikaalinen radar pictures: a)-d) 0.3˚ PPI and e)-h) 4.0˚ VPPI pictures at 1500-1517 UTC. Note the velocity folding at a maximum unambiguous velocity of 22 m/s, and the two minute time difference between reflectivity and velocity data. Circles denote the small scale mesovortices, arrows are pointing to the centre of each vortex. The strong mesovortex discussed in the text is denoted by M. The radar location is marked by a white cross.

The Doppler velocity data had indications of several small scale cyclonic vortices along the cold front, but good measurements were obtained only from the one that passed the closest (10 km) to Ikaalinen radar (M in fig. 4). This mesovortex was co-located with the low level reflectivity gap. The direction of the motion was slightly northward compared to the motion of the rainband itself. Atkins et al. (2004) also found in their study that some of the mesovortices moved in the same direction as bow echoes but some tend to move northwards relatively to the bow echo apex.

The vortex core diameter was 2.5 km at a height of 1 km at 1512 UTC (Fig. 4g) and with differential velocity of 28 m/s. At 1517 UTC, the differential velocity was still 28 m/s, and 22 m/s at 1522 UTC. These diameter and velocity values are comparable to those observed in previous observational and numerical studies (Atkins et al. 2004, Trapp and Weisman 2003). Atkins et al. (2004) observed that non-tornadic mesovortices tend to have differential velocity less than 20 m/s, whereas in tornadic vortices it usually exceeds 25 m/s.

The measured peak velocities may be underestimated, since a small vortex is situated in larger sample size, and the vortex radius overestimated (cf. Brown and Wood 1991). The lower measured velocities further from the radar are probably partly caused by larger sample volumes.

Fig. 1 shows the mesovortex path measured by the radar between 1457-1555 UTC. Four emergency reports were located along the observed path, but no tornado reports were received from there. The tornado report east of the mesovortex track is co-located with the path of the next reflectivity gap southeast of the studied mesovortex (see down right corner of fig. 4c), but due to the distance from the radar and attenuation, good velocity measurements were not obtained. However, the wind damage reports show several longer tracks, which may have been caused by similar vortices. The movements of the reflectivity bulges were fast, so even weak vortices could have caused damage. However, a notable fraction of wind damage reports were probably caused by downbursts. Several recent studies have linked low-level mesovortices to the occurrence of downbursts (e.g. Atkins et al. 2004, Atkins et al. 2005, Wheatley et al. 2006, Järvi et al. 2007).

4.2 Kumpula polarimetric radar observations

As the severe frontal rainband approached Helsinki, the faster moving cold frontal rainband was about to catch up the pre-frontal rainband. The Doppler velocity data (not shown) indicated a south-north oriented mid-level jet with 26-30 m/s maximum winds at about 3 km height in front of the cold front. Another parallel wind maximum (22-26 m/s) existed approximately at 1 km height just in front of the squall line. A westerly rear inflow jet (orange area west of the squall line in Fig. 5b) was observed behind the leading line at about 0.5-1.5 km height.

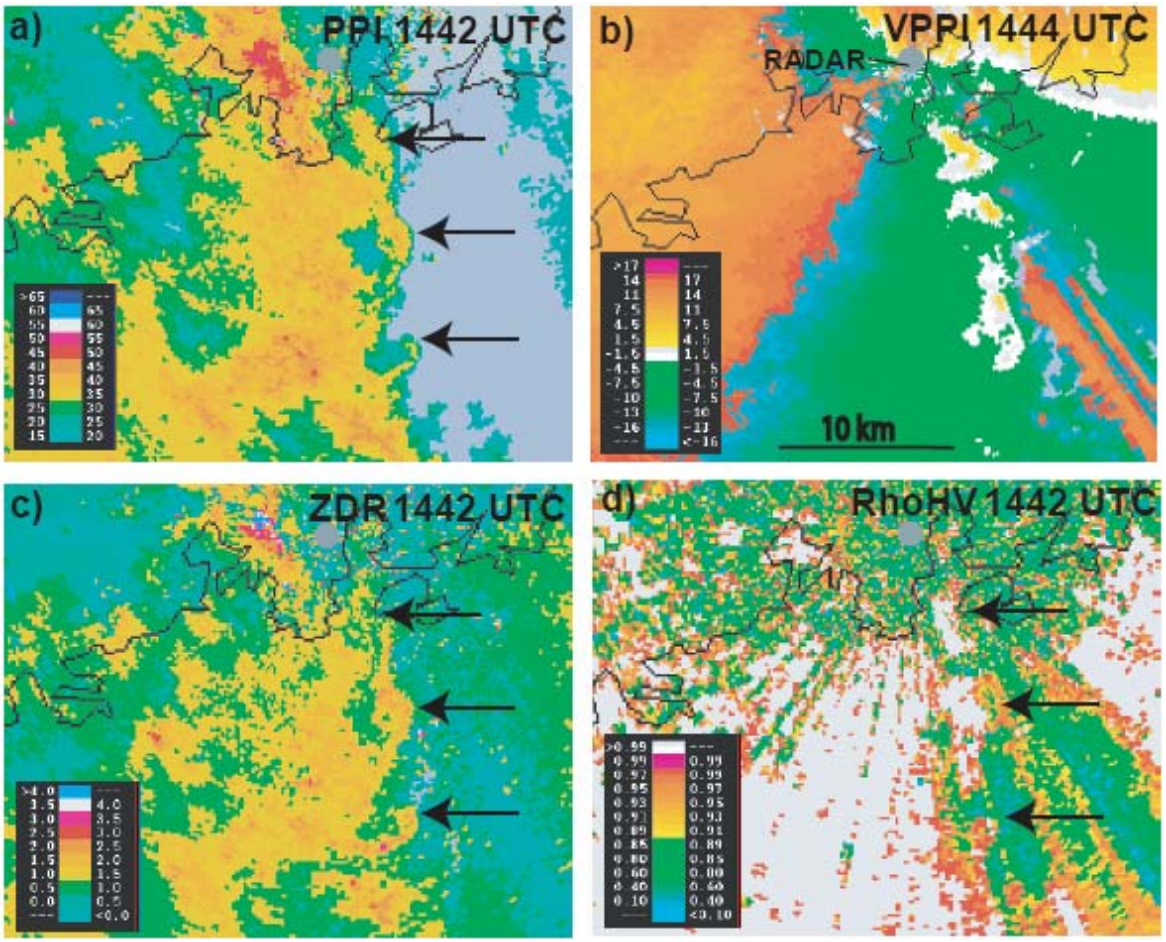

Fig. 5. Kumpula radar pictures: a) 1.2˚ PPI at 1442 UTC b) 2.2˚ VPPI at 1444 UTC (Note the velocity folding at 16 m/s and two minutes time difference compared to other pictures) c) 1.2˚ differential reflectivity ZDR at 1442 UTC and d) 0.3˚ cross-correlation coefficient at 1442 UTC. Arrows indicate the reflectivity hooks.

The rainband seemed to lose its shape and the reflectivities decreased. It had wavelike patterns at two separate scales. At larger scale, a gap in low level reflectivity, similar to the gaps near Ikaalinen radar, was observed somewhat inland from the coast. At smaller scale, reflectivity waves and small reflectivity hooks developed ahead of the approximately 50 km wide bowing segment that moved over southern coast eastward. These reflectivity hooks formed south of the apex of the bowing segment. Tornadoes are more often observed north of the bow echo apex and only a few cases have been documented on its south side (e.g. Atkins et al. 2004, Forbes and Wakimoto 1983, Przybylinski 1995). Atkins et al. (2005) suggested that squall line mesovortices are more likely in becoming tornadic if the gust front is strengthened by a rear inflow jet.

At 1442 UTC, the leading line was over Helsinki (Fig. 5a) and had already weakened in reflectivity. The Doppler velocity data had three small scale vortices over the sea in the leading line (Fig. 5b). The northern vortex, which was closest to the radar (4 km range) is very close to the location where three waterspout observations occurred. This cyclonic vortex had a 2 km core diameter at 200 m height and 24 m/s differential velocity. The vortex could be identified also in the previous radar pictures moving 20 m/s northeast. The path of the vortex continued inland, from where at least 4 emergency reports of fallen trees were received. The two other vortices were at about 5 km intervals south and had similar differential velocities.

The differential reflectivity ZDR (Fig. 5c) showed narrow 1.5-3.5 dB differential reflectivity hooks extending ahead of the rainband with embedded lower values at the tip of the hook at 0.3 and 0.4 km height. These hooks could be identified also at lower elevation. The hooks were co-located with the two southern vortices (Fig. 5b). The northern vortex was co-located with a 2 km diameter ZDR minimum and again higher (1-1.5 dB) values around it. The previous radar pictures along the vortex track (not shown) showed anomalously high ZDR hooks of 3.5-4.0 dB, and locally >4.0 dB. Only the southeast vortex was visible in the cross-correlation coefficient measurements (Fig. 5d) as 1.2 km diameter round

circle of high values surrounding a minimum at 0.2 km height, co-located with the vortex and the tip of the reflectivity hook.

Tornadic debris signatures are characterised by an anomalously low cross-correlation coefficient and differential reflectivity (Ryzhkov et al. (2005). In the Helsinki case, at 1442 UTC the vortices were over water, so one would not expect lofted debris to cause these anomalies. However, the trajectories of different size hydrometeors in the presence of strong circulation may lead to a ZDR-anomaly. Ryzhkov et al. (2005) noticed an anomalously high ZDR comma-shaped signature to wrap the mesoscale vortex. This is expected to happen because smaller hydrometeors are easily re-circulated back to the updraft as big particles fall down despite the updraft. It is possible that the same phenomenon was observed in the ZDR hooks in the Helsinki case. The spiralling rain shaft wrapping around the vortices seen in this case resembles the simulated non-supercell tornadogenesis along an outflow boundary in its mature and dissipation stage (Lee and Wilhelmson 1997a, 1997b). According to the eyewitness report, looking south to the tornado, the visibility was diminished by heavy rain.

5. CONCLUSIONS AND DISCUSSION

A severe frontal rainband developed along a rapidly moving cold front that was preceded by a prefrontal rainband, a strong mid-level jet and nearly saturated low level air having only marginal buoyancy. At larger scale, the leading line reflectivity structure of the frontal rainband had distinct gaps and its reflectivity structure resembles some documented high vertical wind shear cases (e.g. Carbone 1982, Funk et al. 1999) and numerical studies (Weisman and Trapp 2003).

Several mesovortices were detected along the leading line of the rainband. Near the polarimetric radar, south of the 50 km wide bow echo apex (cf. Atkins et al. 2005), the vortices were co-located with the reflectivity hooks (cf. Weisman and Trapp 2003). In addition, differential reflectivity hooks were observed co-located with the radar identified vortex locations near Helsinki.

As noted by Johns (1993), in weak instability dynamic pattern bow echoes, the reflectivities are often very low and appear to have little correlation with the outflow strength. Therefore, he stated that in weak instability bow echo situations, assessing severe weather potential based on reflectivity values is likely not very effective. The bowing segments are not always pronounced (as in this case), or may occur after the onset of severe weather (e.g. Atkins et al. 2005). This is why Funk at al. (1999) suggested issuing blanket warnings for fast-moving squall lines.

These results indicate that the use of Doppler velocity data in Finland would benefit the nowcasting of severe convective weather. However, interesting radar features are usually small in extent in comparison to vast nowcasting areas, so that their recognition would usually require radar algorithms to pinpoint the location of potentially severe convective storms. As shown in this paper, the squall line mesovortices are often well sampled only very close to the radar. Therefore, observations of such vortices somewhere along the squall line should attract the forecasters' attention to downburst or tornado potential. To discriminate between tornadic and nontornadic mesovortices along a quasi-linear convective system, low-level velocity data with high temporal and spatial resolution are needed (Atkins et al. 2005). In Finland also, the unambiguous wind velocity in lower scanning elevations should reach high enough values to avoid velocity folding.

REFERENCES

Atkins, N. T., J. M. Arnott, R. W. Przybylinski, R. A., Wolf, and B. D. Ketcham, 2004: Vortex structure and evolution within bow echoes. Part I: Single-doppler and damage analysis of the 29 June 1998 derecho. *Mon. Wea. Rev.*, **132**, 2224–2242.

Atkins, N. T., C. S. Bouchard, R. W. Przybylinski, R. J. Trapp, and G. Schmocker, 2005: Damaging surface wind mechanisms within the 10 June 2003 Saint Louis bow echo during BAMEX. *Mon. Wea. Rev.*, **133**, 2275–2296.

Brown, R. A., and V. T. Wood, 1991: On the interpretation of single-Doppler velocity patterns within severe thunderstorms. *Wea. Forecasting,* 6, 32-48.

Carbone, R. E., 1982: A severe frontal rainband. Part I: Stormwide hydrodynamic structure. *J. Atmos. Sci.*, **39**, 258-279.

Forbes, G. S., and R. M. Wakimoto, 1983: A concentrated outbreak of tornadoes, downbursts and microbursts, and implications regarding vortex classification. *Mon. Wea. Rev.*, **111**, 220–236.

Funk, T. W., K. E. Darmofal, J. D. Kirkpatrick, V. L. Dewald, R. W. Przybylinski, G. K. Schmocker, and Y.-J. Lin, 1999: Storm reflectivity and mesocyclone evolution associated with the 15 April 1994 squall line over Kentucky and southern Indiana. *Wea. Forecasting,* **14**, 976–993.

Johns, R. H., 1993: Meteorological conditions associated with bow echo development in convective storms. *Wea. Forecasting*, **8**, 294–299.

Järvi, L., A.-J. Punkka, D. M. Schultz, T. Petäjä, H. Hohti, J. Rinne, T. Pohja, M. Kulmala, P. Hari, and T. Vesala, 2007: Micrometeorological observations of a microburst in southern Finland. *Boundary-Layer Meteorology*, **125**, 343-359.

Lee, B. D., and R. B. Wilhelmson, 1997a: The numerical simulation of non-supercell tornadogenesis. Part I: Initiation and evolution of pretornadic misocyclone

circulations along a dry outflow boundary. *J. Atmos. Sci.*, **54**, 32-60.

Lee, B. D., and R. B. Wilhelmson, 1997b: The numerical simulation of non-supercell tornadogenesis. Part II: Evolution of a family of tornadoes along a weak outflow boundary. *J. Atmos. Sci.*, **54**, 2387-2415.

Przybylinski, R. W., 1995: The bow echo: Observations, numerical simulations, and severe weather detection methods. *Wea. Forecasting,* **10**, 203–218.

Ryzhkov, A. V., T. J. Schuur, D. W. Burgess, and D. S. Zrnic, 2005: Polarimetric tornado detection. *J. Appl. Met.*, **44**, 557–570.

Saltikoff, E., W. F. Dabbert, J. Poutiainen, J. Koistinen, and H. Turtiainen, 2005: The Helsinki Testbed: A four-season mesoscale research and development facility. *Preprints, 13th Symposium on Meteorological Observations and Instrumentation*, Savannah, Amer. Meteor. Soc., CD-ROM.

Trapp, R. J, and M. L. Weisman, 2003: Low-level mesovortices within squall lines and bow echoes. Part II: their genesis and implications. *Mon. Wea. Rev.*, **131**, 2804–2823.

Weisman, M. L., and R. J. Trapp, 2003: Low-level mesovortices within squall lines and bow echoes. Part I: Overview and dependence on environmental shear. *Mon. Wea. Rev.*, **131**, 2779–2803.

Wheatley, D. M., R. J. Trapp, and N. T. Atkins, 2006: Radar and damage analysis of severe bow echoes observed during BAMEX. *Mon. Wea. Rev.*, **134**, 791–806.